DOI:10.22337/2587-9618-2023-19-3-114-129

NUMERICAL MODELLING OF WIND LOADS ON WINDOWS. VALIDATION FOR A HIGH-RISE SQUARE PLAN BUILDING

Oleg S. Goryachevsky

National Research Moscow State University of Civil Engineering, Moscow, RUSSIA

Abstract: This paper presents the results of numerical and experimental modelling of mean and peak pressure coefficients for window assemblies on a rectangular building. The applicability of the SST and GEKO *k*-ω turbulence models implemented in ANSYS Fluent is investigated. A simple steady-state method for determining the peak wind pressures, which utilizes the turbulence kinetic energy calculation, is shown to be sufficient for practical purposes. A comparative analysis with the values of pressure coefficients given in the Russian building code is carried out. The obtained results can be used in the design of window assemblies of typical buildings.

Keywords: computational fluid dynamics (CFD), experimental wind tunnel (WT) testing, pressure coefficients, structural aerodynamics, window assemblies

ЧИСЛЕННОЕ МОДЕЛИРОВАНИЕ ВЕТРОВЫХ ДАВЛЕНИЙ НА ОКНА. ВАЛИДАЦИЯ ДЛЯ ТИПОВОГО МНОГОЭТАЖНОГО ЗДАНИЯ КВАДРАТНОЙ ФОРМЫ

О.С. Горячевский

Национальный исследовательский Московский государственный строительный университет, г. Москва, РОССИЯ

Аннотация: В статье представлены результаты численного и экспериментального моделирование средних и пиковых аэродинамических коэффициентов для оконных конструкций прямоугольного здания. Исследуется применимость моделей турбулентности SST и GEKO *k*-ω, реализованных в программном комплексе ANSYS Fluent. Показана достаточная для практических целей точность стационарной постановки и простейшего метода определения пиковых значений ветровых давлений на основе кинетической энергии турбулентности. Проведен сопоставительный анализ со значениями аэродинамических коэффициентов, приведенных в российских нормах. Полученные результаты могут быть использованы при проектировании оконных конструкций типовых зданий.

Ключевые слова: вычислительная гидродинамика, экспериментальные испытания в аэродинамической трубе, аэродинамический коэффициент давлений, строительная аэродинамика, оконные конструкции

1. INTRODUCTION

Physical (experimental) modelling of wind loads and actions took on in its modern form in the middle of the 20th century. Tests in wind tunnels (WTs) with uniform flow began in the early 20th century [1], but the results differed significantly from field observations. The first WT with a long test section used to model atmospheric boundary layer (ABL) was built at the Colorado A&M College campus [2]. The first significant structures that were designed based on test results from the same WT (the college had already been renamed to Colorado State University) were the World Trade Centre Twin Towers in 1964 [3-4].

Large-scale studies were conducted for another 30 years to test against the full-scale (field) data in order to validate the experimental modelling results [5-10]. Important validation requirements were identified, including the reproduction of the statistical flow characteristics (mean velocities, turbulence intensity and spectrum)

[11-13], taking into account the developed similarity criteria [14] and the use of high-frequency pressure sensors [15]. Limitations were also identified, e.g., the Reynolds number independence is observed only for bluff bodies, and the deviation from field data for roofs and bodies with uncertain separation point. A review of the history of development and validation of experimental modelling of wind actions is given in [16].

Computational Fluid Dynamics is a powerful tool for analyzing wind actions and related problems (pedestrian comfort, emission propagation, snow loads, etc.) [17-18].

The first works on numerical modelling of wind actions were carried out in the 1970s. However, mass industrial application of CFD technologies was hampered by [19]:

1) colossal requirements for computational resources at the time;
2) insufficient theoretical development of turbulence models and eddy-resolving approaches;
3) lack of software available to the researching engineers;
4) lack of reliable V&V process.

Due to scientific and technological progress, by the beginning of the 21st century, favourable opportunities for industrial application of CFD technologies in the construction industry have developed. Therefore, in the early 2000s there was an explosive growth in the number of scientific studies and attempts (successful and not) to apply, verify and validate numerical modelling for the solution of problems of structural aerodynamics [20-23]. The first CFD application guidelines in structural aerodynamics from European [24] and Japanese [25] researchers were published. They contained basic recommendations for boundary conditions, size of the computational domain, turbulence models, discretization parameters, reliable numerical schemes and V&V principles.

At present, there are a number of building code recommendations on the application of computational fluid dynamics in structural aerodynamics, including the determination of wind loads [26-29]. Meanwhile, contrary to the global trend, numerical modelling of wind loads and actions has been removed from the Russian building code [30].

Among Russian-language sources, there is a deficit of high-quality literature on numerical modelling of wind actions in structural aerodynamics. The only full-fledged monograph exists [31], and the papers on modelling snow loads [32], aeroelasticity of buildings and structures [33] and estimation of pedestrian comfort parameters [34] are noteworthy.

There are three main approaches to the numerical solution of the Navier-Stokes equations [35-36]:

1) DNS (Direct Numerical Simulation), which is characterized by extremely high computational complexity, relevant only for academic problems at low Reynolds numbers;
2) LES (Large Eddy Simulation), which is used to determine transient characteristics of the flow. It has high computational complexity when the wall functions are used and even higher complexity when the boundary layer is resolved;
3) RANS (Reynolds-averaged Navier-Stokes), which is a fast but often insufficiently accurate approach for determining time-averaged flow characteristics.

In industrial applications, the hybrid RANS-LES approach [37] shows sufficiently accurate results with adequate requirements to computational resources.

With any approach utilized, the reliability of the obtained results is evaluated after V&V procedure of the numerical model against the experimental data [38]. An integrated approach with simultaneous use of numerical and experimental modelling results gives a synergistic effect, eliminating the weaknesses of each approach [39].

Based on qualitative experimental results, it is possible to calibrate the parameters of numerical models (usually, the coefficients of turbulence models) to obtain reliable and more

comprehensive results. Recently, the GEKO *k*-ω turbulence model has been developed, which makes it relatively easy to calibrate its parameters using experimental data [40-41].
This paper presents the results of numerical modelling of mean and peak pressure coefficients on the facades of a rectangular 25-storey building. The results of numerical modelling were compared to the experimental data obtained in the WT of NRU MSUCE for the corresponding building and the normative values of SP 20 [30].

2. METHODOLOGY

2.1. Building model description

The mean and peak pressure coefficients on the façade windows of a rectangular 25-storey building are investigated (Fig. 1). The building dimensions are $d \times d$=40×40*m*, and the height is h = 75*m*. Windows' dimensions are 1.75×2*m*, and the spacing is 2.958*m*. Depth of windows in the façade is 0.23*m*.

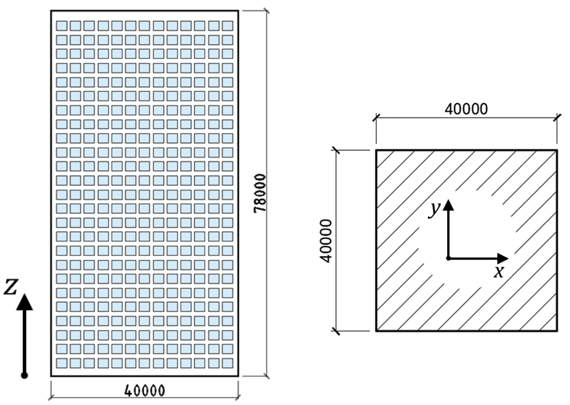

a) front view *b) top-down view*

Figure 1. *Building dimensions, mm*

Numerical modelling and wind tunnel tests were performed for 24 wind directions (from 0° to 345° in 15° intervals) (Fig. 2). The model's symmetry allowed to reduce the number of sensors and to estimate the modelling errors.

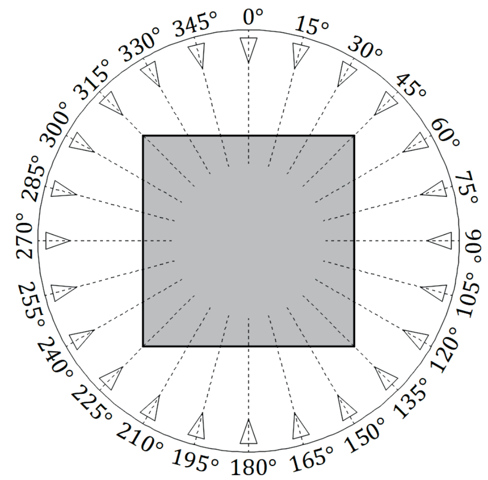

Figure 2. *Design wind directions*

Pressure coefficients were measured at the centroids of the window surfaces. Since each window is an independent structure, the extreme values of pressure coefficients are of practical interest:

$$c_e^{\max} = \max_j \left(c_e^j \right); \quad c_e^{\min} = \min_j \left(c_e^j \right)$$
$$c_{e,+}^{\max} = \max_j \left(c_{e,+}^j \right); \quad c_{e,-}^{\min} = \min_j \left(c_{e,-}^j \right) \tag{1}$$

where c_e^j is the external mean pressure coefficient for the j-th wind direction, and $c_{e,+(-)}^j$ is the external positive (negative) peak pressure coefficient for j-th wind direction.

2.2. Wind pressure coefficients

Pressure coefficients at the building surfaces were determined in the classical way:

$$c\left(x, y, z\right) = \frac{\Delta P(x, y, z)}{Q(h)} \tag{2}$$

where c is the generalized pressure coefficient, ΔP is the excessive wind pressure on the building façade, Q is the dynamic pressure, and x, y, z are the coordinates.
In SP 20, the pressure coefficients vary only horizontally, and the vertical variability is controlled by the equivalent height z_e [30]. Therefore, in order to accurately compare the

values of the coefficients given in SP 20 to those modelled numerically or in the WT (2), it is necessary to take into account the following relationship between them:

$$c = \frac{\Delta P}{Q} = \frac{w_0 k(z_e) c_{norm}}{w_0 k(h)} = \\ = c_{norm} \left(\frac{z_e}{10}\right)^{2\alpha} \Big/ \left(\frac{h}{10}\right)^{2\alpha} = c_{norm} \left(\frac{z_e}{h}\right)^{2\alpha} \quad (3)$$

where w_0 is the basic wind pressure, $k(z_e)$ is the height variation factor, α is the terrain factor, and c_{norm} are the values of horizontal pressure coefficients given in SP 20.
For the object of this study:

$$z_e = \begin{cases} d, & 0 < z < h - d \\ h, & z \geq h - d \end{cases} \quad (4)$$

Then:

$$c = \begin{cases} c_{norm} \left(d / h\right)^{2\alpha}, & 0 < z < h - d \\ c_{norm}, & z \geq h - d \end{cases} \quad (5)$$

As can be seen from expression (5), starting from the 13th floor and above, the values of pressure coefficients according to (2) and the building code are identical. Consequently, for the upper floors the numerical and experimental values can be compared directly. For a correct comparison of values on the lower floors it is necessary to lower the normative coefficients by a factor of 0.82, 0.77 and 0.72 for terrain types A, B and C respectively.
It should be remembered that the piecewise-constant vertical values of wind pressures given in SP 20 [30] are a simplification. In reality, the pressure coefficients are distributed over the surface continuously, forming complex three-dimensional patterns (Fig. 4). Value jumps can be observed only across the corners.

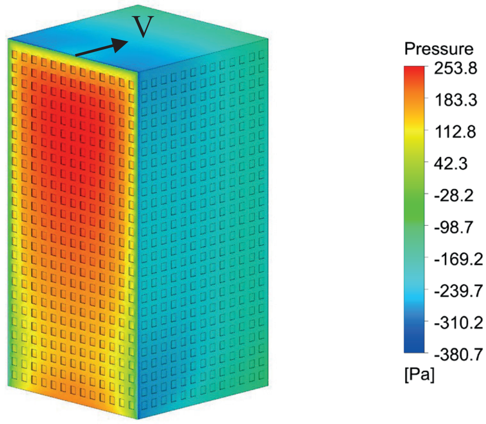

Figure 3. Numerical simulation of mean wind pressure distribution, Pa

2.3. Wind tunnel experiment description

Experimental studies were carried out in the NRU MSUCE WT by the AAISK UNPL staff. The WT has a closed circuit and a modular nine-unit fan with a testing area length of 18.9*m*.
The upstream flow velocities and reference pressures were determined 1.5*m* away from the 1:100 scale model placed in the WT testing area (Fig. 4).
Pressure sensors were placed in the middle of window openings on the 14th, 23rd and 25th floors (Fig. 5) on two sides of the model.
Pressure coefficients for each control point and wind direction were determined by statistical processing of pressure sensor readings (1000Hz frequency):

$$c_e = \frac{\Delta P_{ave}}{Q} \\ c_{e,+(-)} = \frac{\Delta P_{max(min)}}{Q} \quad (6) \\ P_{max(min)} = \Delta P_{ave} \pm 3\sigma_P$$

where ΔP_{ave}, ΔP_{max}, ΔP_{min} are average, maximum and minimum pressure values at the test points, respectively, σ_P is the wind pressure standard deviation, and Q is the dynamic pressure at the top of the model.

The experiments were carried out without roughness, as the aim was to determine the pressure coefficients with the least influence of the upstream flow turbulence possible.

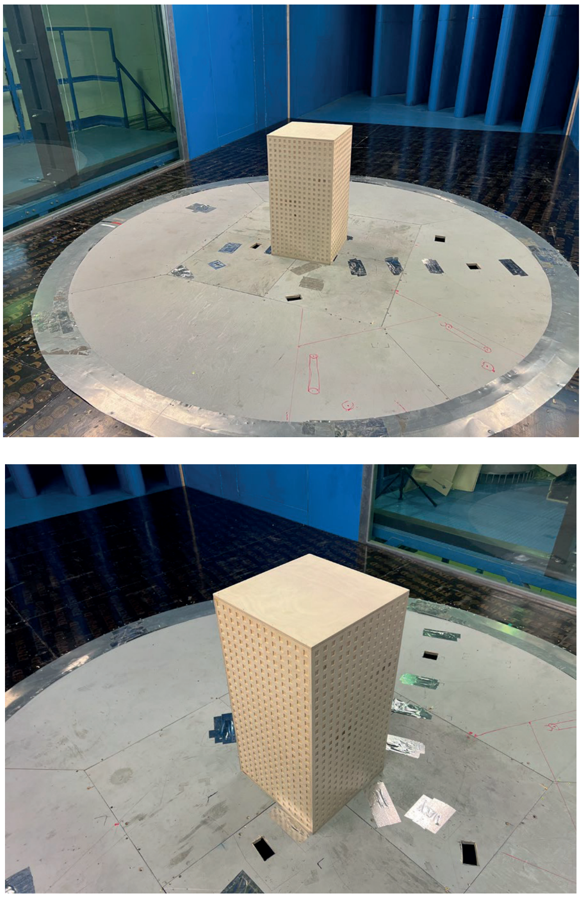

Figure 4. Building model in the WT

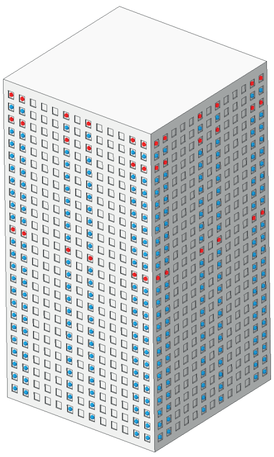

Figure 5. Pressure sensors (in red, not present on the other sides) and additional measurement points in the numerical model (in blue, present on all sides) layout

2.4. Numerical model description

The numerical model is based on the Navier-Stokes equations for incompressible Newtonian fluid with mass forces omitted:

$$\frac{\partial u_i}{\partial t} + u_j \frac{\partial u_i}{\partial x_j} = -\frac{1}{\rho}\frac{\partial p}{\partial x_i} + \frac{\mu}{\rho}\frac{\partial^2 u_i}{\partial x_i \partial x_j}; \qquad \frac{\partial u_i}{\partial x_i} = 0; \quad \rho, \mu = \text{const} \tag{7}$$

where u_i is the velocity components for the x_i direction, p is the pressure, ρ is the density, μ is the dynamic viscosity, and t is the time.

Direct numerical solution of equations (7) for practical problems at high Reynolds numbers is not possible due to very high computational requirements. LES approach is not considered in this paper, as well. In the present study, the Reynolds-averaged Navier-Stokes (RANS) equations are applied, obtained by decomposing the instantaneous quantities into their time-averaged and fluctuating quantities:

$$\boldsymbol{u}(\boldsymbol{x},t) = \overline{\boldsymbol{u}}(\boldsymbol{x}) + \boldsymbol{u}'(\boldsymbol{x},t) \qquad p(\boldsymbol{x},t) = \overline{p}(\boldsymbol{x}) + p'(\boldsymbol{x},t) \tag{8}$$

where $\boldsymbol{u}'(\boldsymbol{x},t)$, $p'(\boldsymbol{x},t)$ are the fluctuating quantities of velocity and pressure, respectively.

The resulting expressions are called the Reynolds equations:

$$\rho \overline{u}_j \frac{\partial \overline{u}_i}{\partial x_j} = \frac{\partial}{\partial x_j}\left[-\overline{p}\delta_{ij} + \mu\left(\frac{\partial \overline{u}_i}{\partial x_j} + \frac{\partial \overline{u}_j}{\partial x_i} \right) - \rho\overline{u_i'u_j'} \right] \tag{9}$$

The disadvantage of time-averaging is the appearance of second order moments $\rho\overline{u_i'u_j'}$ in (9). The additional unknown quantities form the Reynolds stress tensor. To close the obtained equations (9), the additional hypotheses called the turbulence models are needed.

In this paper, two turbulence models are applied:

1) SST, which is widely used and proven in engineering applications [35];

2) GEKO k-ω, which is relatively recently implemented in ANSYS Fluent [40] with wide calibration possibilities.

Let us provide a mathematical description of the latter model:

$$\rho\frac{\partial(\bar{u}_j k)}{\partial x_j} = P_k - C_\mu \rho k\omega + \\ +\frac{\partial}{\partial x_j}\left[\left(\mu+\frac{\mu_t}{\sigma_k}\right)\frac{\partial k}{\partial x_j}\right] \quad (10)$$

$$\rho\frac{\partial(\bar{u}_j \omega)}{\partial x_j} = C_{\omega 1}F_1\frac{\omega}{k}P_k - C_{\omega 2}F_2\rho\omega^2 + \\ +\rho F_3 CD+\frac{\partial}{\partial x_j}\left[\left(\mu+\frac{\mu_t}{\sigma_\omega}\right)\frac{\partial \omega}{\partial x_j}\right] \quad (11)$$

where k is the turbulence kinetic energy (TKE), ω is the specific turbulence dissipation rate, P_k is the production of TKE, $\mu_t = \rho k/\omega$ is the eddy viscosity, $CD = \frac{2}{\sigma_\omega}\frac{1}{\omega}\frac{\partial k}{\partial x_j}\frac{\partial \omega}{\partial x_j}$, C_μ, $C_{\omega 1}$, $C_{\omega 2}$, σ_k, σ_ω are the model constants, and F_1, F_2, F_3 are the model functions, which can be calibrated through freely assignable coefficients. In this work, the value of $C_{SEP}(F_1, F_2, F_3)$, which governs the eddy viscosity, was varied. The values of C_{SEP} = 1.00, 1.75 and 2.25 were considered.

Note that k-ω models have a weakness in modelling the free shear flows because of the strong dependence on the inlet turbulent characteristics [42]. Therefore, in practice, mixed BSL-SST models are used, which implement both k-ε and k-ω models in different flow regions. The separation of the regions is done by blending functions. The GEKO k-ω model implements a similar approach.

The following boundary conditions for the computational domain were applied:

1) the velocity profile at the inlet: $(\bar{\boldsymbol{u}},\boldsymbol{n}) = U(z), (\bar{\boldsymbol{u}},\tau) = 0$ ($\boldsymbol{n}$, $\boldsymbol{\tau}$ are vectors normal and tangent to the surface, respectively, z is the height coordinate);

2) $k(z)$ and $\omega(z)$ were also specified at the inlet;

2) backflow pressure at the outlet was set to 0: $\bar{p} = 0$;

3) free slip wall conditions were set for the lateral and upper boundaries: $(\bar{\boldsymbol{u}},\boldsymbol{n}) = 0, (\bar{\boldsymbol{u}},\boldsymbol{n}) = 0$;

4) no-slip wall conditions were set for the ground and building surfaces: $\bar{\boldsymbol{u}} = 0$.

The standard (RMS) wind pressures were calculated using the methodology that is outlined in [31]:

$$\Delta\bar{p}+\sigma_P = \frac{\rho}{2}\left(\bar{U}+\sigma_U\right)^2$$

$$\sigma_P = \frac{\rho}{2}\left(2\bar{U}\sigma_U+\sigma_U^2\right)$$

$$\sigma_P = \left[2\frac{\sigma_U}{\bar{U}}+\left(\frac{\sigma_U}{\bar{U}}\right)^2\right]\Delta\bar{p}$$

$$\sigma_P = \left(2I_U+I_U^2\right)\Delta\bar{p} \quad (12)$$

where $\bar{U}$ is the mean wind speed, and I_U is the turbulence intensity.

In [31], the turbulence intensity is proposed to be determined from the Bernoulli's law and the turbulence isotropy:

$$I_U = \frac{\sigma_U}{\bar{U}} = \sqrt{\frac{2}{3}k} \div \sqrt{\frac{2|\Delta\bar{p}|}{\rho}} = \sqrt{\frac{\rho k}{3|\Delta\bar{p}|}}, \quad (13)$$

On the walls, the TKE value is 0. Therefore, averaged values are taken in small volumes around the wall points.

The peak pressure coefficients, then, can be estimated by the following formulas:

$$c_{e,+} = \frac{\Delta\bar{p} + \theta_+ \sigma_P}{Q}$$
$$c_{e,-} = \frac{\Delta\bar{p} - \theta_- \sigma_P}{Q} \qquad (14)$$

where θ+, θ- are the coefficients that can be fitted from experimental data (equal for the whole model).

Although expression (13) and the methodology for determining TKE on the walls have somewhat weak theoretical justification, in practice it allows to determine the peak pressure coefficients fairly accurately. This will be confirmed in the present study.

2.5. Numerical simulation description

ANSYS Fluent 2021R2 was used for numerical modelling, carried out at a 1:100 scale (k_s = 100), similarly to the WT experiments.

The computational domain size corresponds to a fragment of the WT testing area, with the height of 2.44*m*, width of 4*m* and length of 9.5*m* (Fig. 6). The inlet boundary is located 3*m* away from the center of the building model.

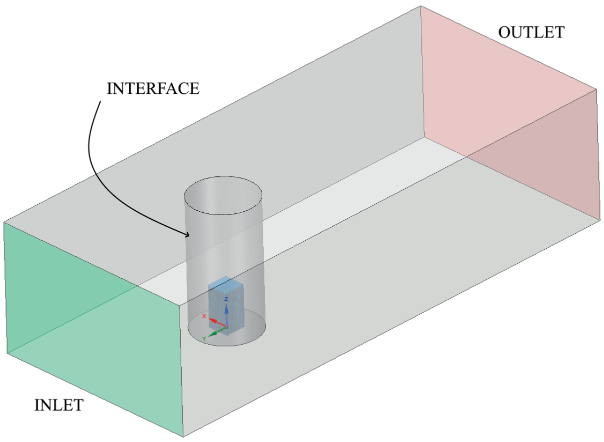

Figure 6. Computational domain

A mesh interface was established between and additional cylindrical volume around the building model and the rest of the domain, approximating the transition between non-conformal meshes. This approach avoids rebuilding the mesh between the wind direction changes, which are achieved by rotating the outer volume around the cylindrical inner volume.

The poly-hexcore finite volume mesh was created in ANSYS Fluent Meshing (Fig. 7). The cell size on the building surface is 0.0025*m* with 5 inflation layers, and the total number of finite volume cells is 5.75 million.

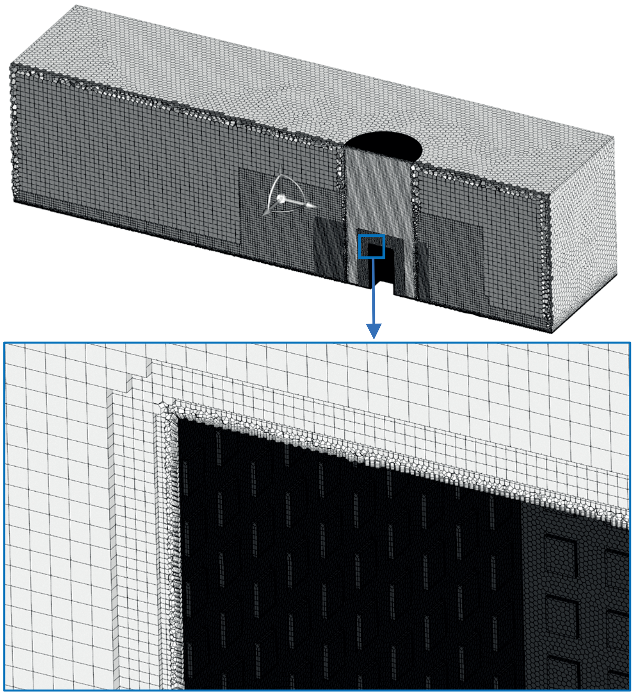

Figure 7. Finite volume mesh section

The simulations were carried out using the steady-state pseudo-transient approach, in which the transient quantities that disappeared after the time-averaging procedure are re-introduced into the equations (9-11). The time, then, is replaced by a sufficiently large pseudo-transient timestep. The relaxation coefficients ensure sufficiently fast convergence. This approach is usually more efficient compared to the direct solution of the steady-state equations.

The total number of iterations is 125. The first 75 iterations are simulated with the standard pseudo-timestep, and the last 50 iterations are simulated with a timestep reduced by a factor of 2. This approach ensures better convergence. At the end of the simulation, the scaled residuals for all conservation equations fall below $5 \cdot 10^{-4}$. Test simulations showed that increasing the number of iterations does not affect the result significantly.

Second Order Upwind numerical scheme was used for the momentum equations (9) and turbulence transport (10-11) in space and pseudo-time. The Coupled pressure-velocity solver was used.

2.6. Inlet profile characteristics

The wind speed profile (Fig. 8) and turbulence characteristics for the inlet were set similarly to those measured in the WT. The expression for wind speed was determined using the least squares method:

$$U(z) = \begin{cases} U_0 \left(z/z_0 \right)^{\alpha}, & z < z_1 \\ U_0 \left(z_1/z_0 \right)^{\alpha}, & z \geq z_1 \end{cases} \qquad (8)$$

where $U_0 = 15.6$m/s, $z_0 = 0.15$m, $z_1 = 0.32$m, $\alpha = 0.10$.

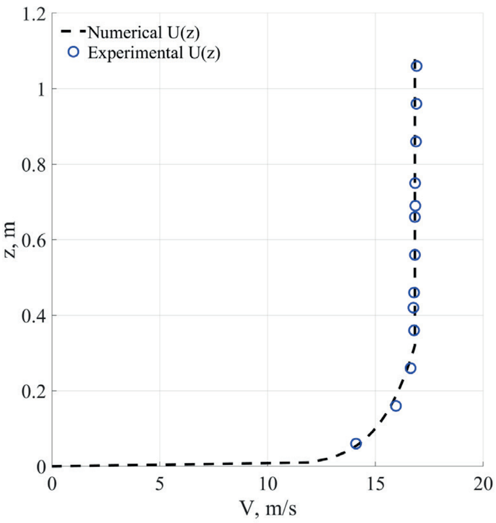

Figure 8. Numerical and experimental wind profiles

The turbulence intensity in the WT was kept constant at ~3% for $z > 0.3$m. For the numerical model, the intensity measured in the experiment was approximated by the least squares method, too. It was then converted to k and ω, which were set at the inlet.

3. RESULTS AND DISCUSSION

For the modelled pressure coefficients, errors were evaluated. For the experimental data, the errors mainly come from deviations in the wind direction angle due to the imperfection of the WT's rotary table mechanism, minor asymmetry in the sensors' location, and sensor measurement errors.

The scatter of experimental values was estimated by the difference between the results obtained in symmetrical zones.

For the numerical data, the errors mainly come from non-ideal iterative convergence and high gradients in the corner zones. Iterative fluctuations were considered for the last 25 iterations. The difference of the sought values was measured on a circular area with a radius of 5*mm* (approximately 30% of the window surface area).

Figs. 9-12 show floor plots of the extreme pressure coefficients' values (1). Each plot includes a diagram, which shows the location of the corresponding windows on the building. The variation of experimental values is shown by error bars, while the variation of numerical values is shown by translucent bars of the appropriate colour.

The SST and GEKO k-ω (C_{SEP} = 1.00, 1.75 and 2.25) turbulence models were considered. The coefficients in expression (14) were taken equal to θ+ = 0.25 and θ- = 2.25.

It is known that the pressure coefficients obtained from numerical simulation are often slightly higher than those from the experiments. This situation is observed even when the reference pressures are measured at the same location. In this study, the shift effect was also detected. Therefore, a correction of the pressure coefficients by $c_{e,shift}$ = 0.07 was introduced to reduce the numerical values.

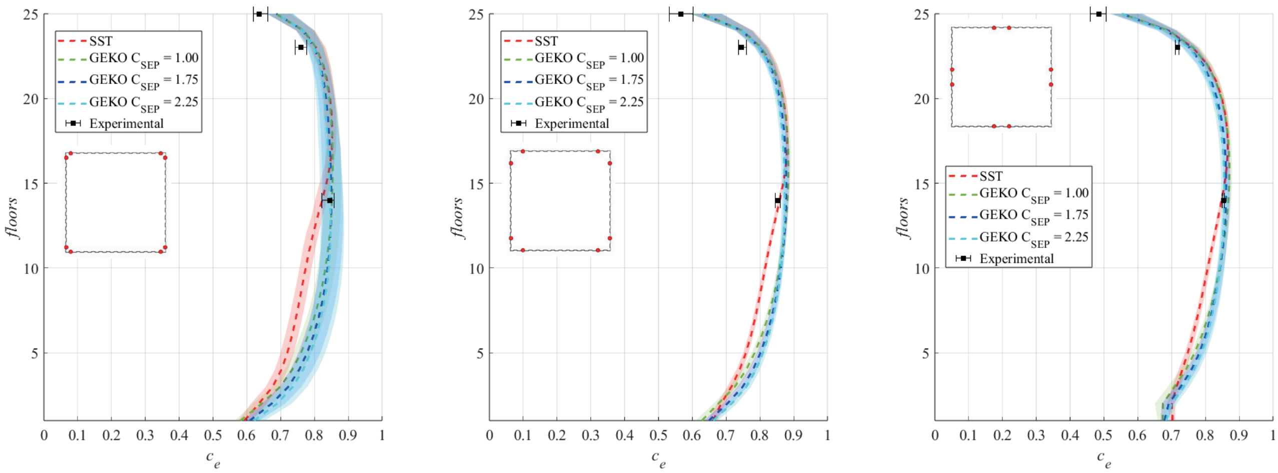

Figure 9. Floor plots of maximum positive values of mean pressure coefficient c_e^{max}

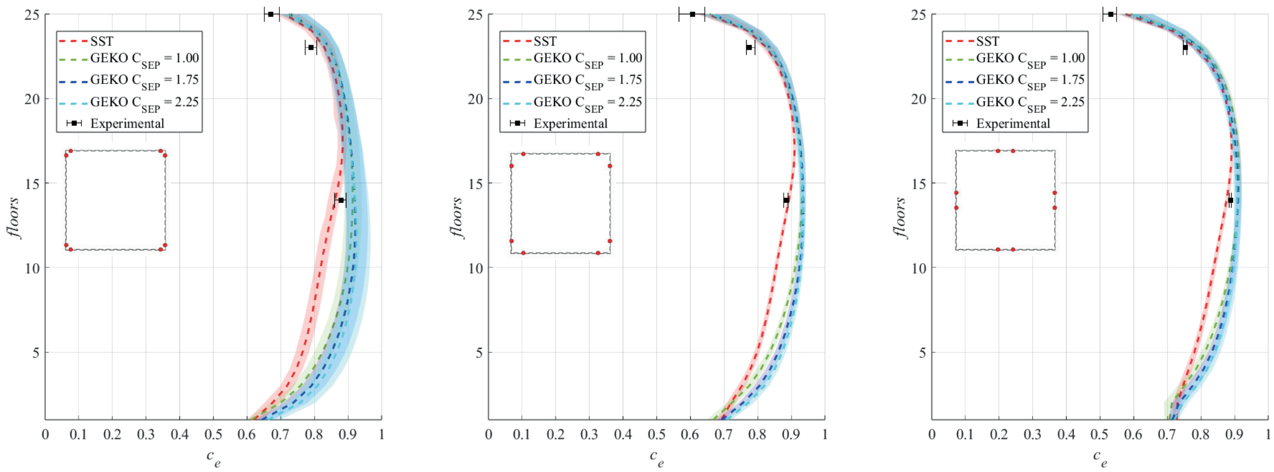

Figure 10. Floor plots of maximum positive values of peak pressure coefficient $c_{e,+}^{max}$

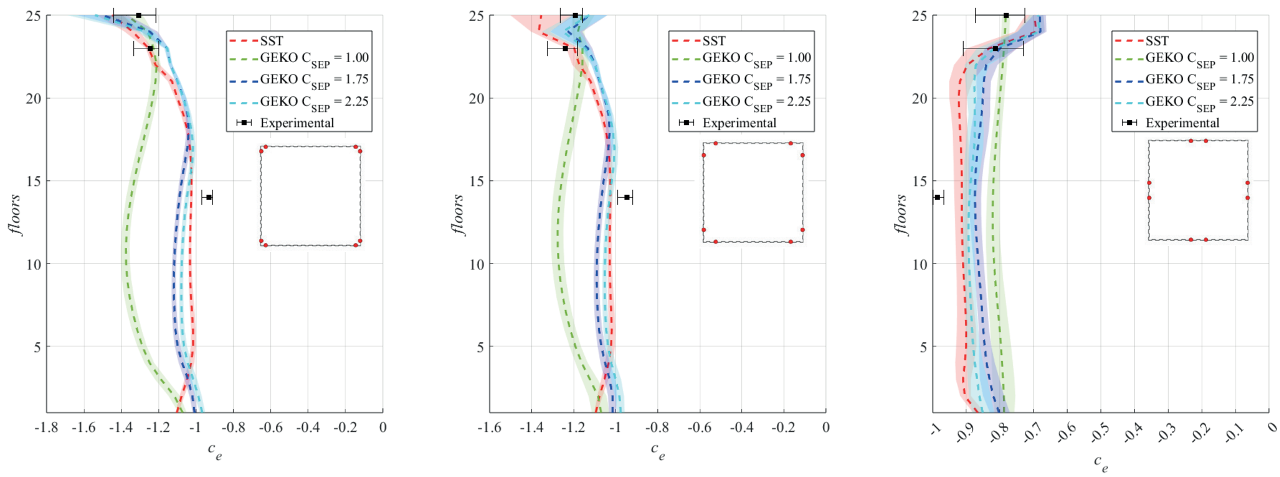

Figure 11. Floor plots of minimum negative values of mean pressure coefficient c_e^{min}

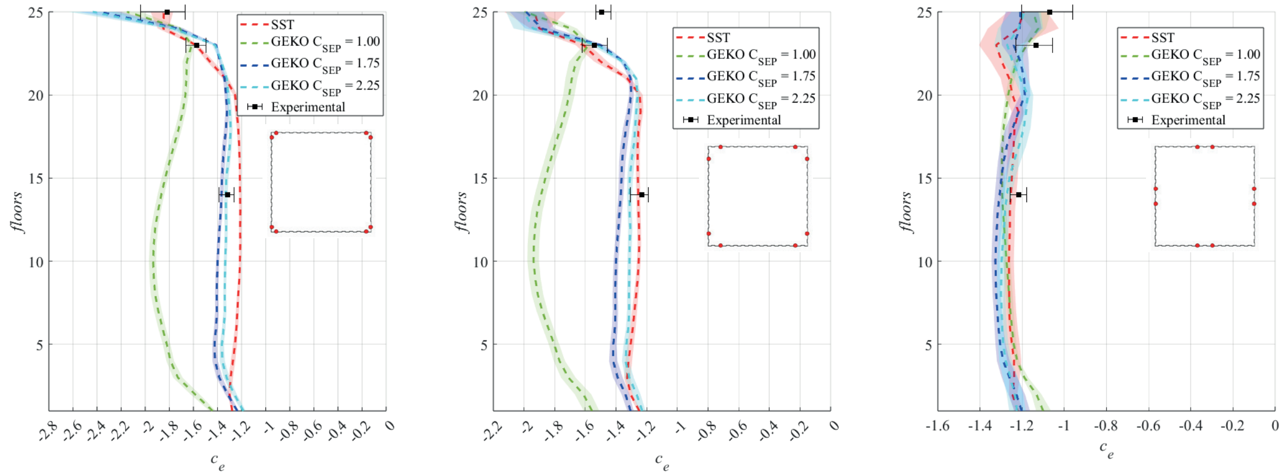

Figure 12. Floor plots of minimum negative values of peak pressure coefficient $c_{e,-}^{\min}$

Analyzing the plots in Figs. 9-12, it can be seen that the numerical and experimental results are subject to noticeable errors. Accounting for the errors allows for a more complete analysis of the results.

1. All numerical and experimental values of $c_e^{\max}$ are in good agreement with each other (deviations <10%). For the floors below the middle one, the SST model gives slightly lower values than GEKO. However, it is not possible to establish which model is more plausible due to the lack of experimental data points.
2. All numerical and experimental values of $c_{e,+}^{\max}$ are in good agreement with each other (deviations <10%). The SST model gives slightly better results than GEKO.
3. The numerical values of $c_e^{\min}$ are significantly different between the turbulence models. GEKO at C_{SEP} = 1.00 gives the worst results (deviation from the experimental data up to 40%) for the 14th floor, but better results for the 23rd and 25th floors (fits within the experimental spread). The SST model gives the best results for the 14th floor (deviation <10%).
4. The numerical and experimental values of $c_{e,-}^{\min}$ are in good agreement with each other in the center zone of the building. However, the SST model gives slightly better results at the 14th floor, while GEKO at C_{SEP} = 1.00 gives better results at the 23rd and 25th floors.
5. In the corner zones, the numerical and experimental values of $c_{e,-}^{\min}$ correspond best for the SST model. However, the experimental data on the 25th floor for the 2nd window from the corner was not reproduced accurately enough by either turbulence model. For this point, the numerical data gives significantly overestimated values (-2.0 vs. -1.5 experimental values).

Comparison of the obtained results with paragraph B.1.17 of SP 20 [30] reveals a significantly poor design of normative schemes (Fig. 13). As such, experimental and numerical values of $c_{e,+}^{\max}$ do not reach even 1.0 anywhere, unlike the value of 1.2 the building code suggests. For the lower and upper parts of the building the values of the coefficients are much lower than for the central part.

At the corners of the 25th floor the numerical values of $c_{e,-}^{\min}$ can reach -2.6 (in the code: -2.2), although the experimental values do not exceed -2.05 (remember that this is where numerical and experimental values deviate the most). However, on other floors, $c_{e,-}^{\min}$ values are significantly lower than normative values. For the 2nd window from the corner, both experimental and numerical values are significantly higher than the normative -1.2. For other zones of the building, $c_{e,-}^{min}$ values can be slightly higher than -1.2, reaching -1.4 in the numerical simulations.

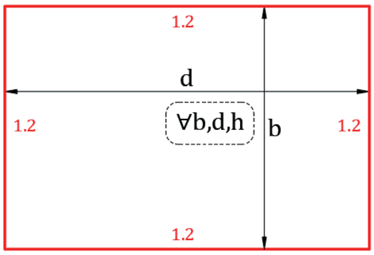

a) $c_{e,+}^{max}$

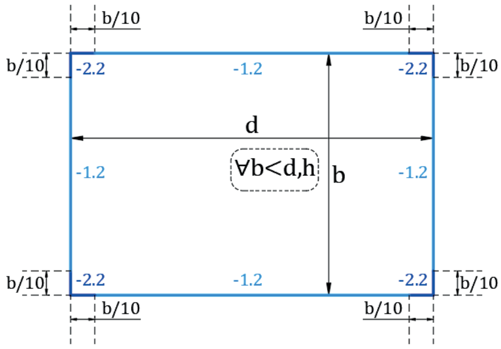

b) $c_{e,-}^{min}$

Figure 13. *Normative values of peak pressure coefficients (h is the building height)*

According to SP 20 [30], the pressure coefficients and the corresponding wind loads decrease steeply at the bottom of the building. However, the modelling results show that the decrease of pressure coefficients at the bottom of the building is observed only for c_e^{max} and $c_{e,+}^{max}$, while c_e^{min} and $c_{e,-}^{min}$ remain almost constant.

The Russian building code does not contain regulations for extreme values of mean pressure coefficients, despite their necessity for the design of window assemblies. Therefore, it is not possible to carry out an appropriate comparison.

4. CONCLUSION

Comparison of the results of numerical and experimental modelling confirms that the numerical modelling of mean and peak wind loads is sufficiently reliable for practical purposes. At the same time, the possibility of numerical modelling to obtain a significantly more complete distribution of the coefficients without additional resources is demonstrated.

One of the important advantages of the proposed approach is the relatively low computational cost due to the use of the steady-state approach only. This is very important for practical problems constrained by time and budget.

However, the numerical approach used in this paper turns out to be dependent on the availability of experimental data for calibrating the turbulence models, computing the coefficients θ+, θ- and the shift factor $c_{e,shift}$. Obviously, the development of more advanced models to determine peak wind pressures independent of experimental data is required.

The GEKO *k*-ω turbulence model has shown a good ability to be calibrated with experimental data. However, to achieve better results than those obtained using the SST model, more research is required for a full calibration of the GEKO model.

The importance of error evaluation for the experimental and numerical results is demonstrated. In industrial applications and scientific research, appropriate analysis is often not performed, which can lead to dangerous underestimation of wind loads.

The extreme values of mean and peak pressure coefficients obtained in this study are recommended for use by window assembly engineers.

REFERENCES

1. **Kazakevich M.I.** Aerodinamika inzhenernyh sooruzhenij. Moscow: OAO Giprotroymost, 2014, 168 p. (in Russian)

2. **Cermak J.E., Koloseus H.J.** Lake Hefner Model Studies of Wind Structure and Evaporation. Final Report – Part II, № 54JEC22, 1954, 123 p.
3. **Davenport A.G.** The response of supertall buildings to wind // Second Century of the Skyscraper: Council on Tall Buildings and Urban Habitat, 1988, pp. 705-725.
4. **Glanz J., Lipton E.** City in the Sky: The Rise and Fall of the World Trade Center. Times Books, 2014, 480 p.
5. **Rathbun J.C.** Wind forces on a tall building // Trans. Am. Soc. Civil Eng., 1940, Volume 105, pp. 1-41.
6. **Marshall R.D.** A study of wind pressures on a single-family dwelling in model and full scale // J. Wind Eng. Ind. Aerodyn., 1975, Volume 1, pp. 177-199.
7. **Eaton K.J., Mayne J.R.** The measurement of wind pressures on two-storey houses at Aylesbury // J. Wind Eng. Ind. Aerodyn., 1975, Volume 1, pp. 67-109.
8. **Holmes J.D.** Comparison of model and full-scale tests of the Aylesbury house // Proceedings of the International Workshop on Wind Tunnel Modeling Criteria and Techniques in Civil Engineering Applications, 1982, pp. 605-618.
9. **Richardson G.M., Robertson A.P., Hoxey R.P., Surry D.** Full-scale and model investigations of pressures on an industrial/agricultural building // J. Wind Eng. Ind. Aerodyn., 1990 ,Volume 36(2), pp. 1053-1062.
10. **Hoxey R.P., Richards P.J.** Full-scale wind load measurements point the way forward // J. Wind Eng. Ind. Aerodyn, 1995, Volume 57, Issues 2-3, pp. 215-224.
11. **Monin A.S., Obukhov A.M**. Basic laws of turbulent mixing in the surface layer of the atmosphere // Contrib. Geophys. Inst. Acad. Sci. USSR, 1954, Volume 24(151), pp. 163-187 (in Russian).
12. Van der Hoven I. Power spectrum of horizontal wind speed in the frequency range from 0.0007 to 900 cycles per hour // Journal of Atmospheric Sciences, 1957 Volume 14, pp. 160-164.
13. **Davenport A.G.** The relationship of wind structure to wind loading // Proc. Conf. on Wind Effects on Buildings & Structures, HMSO, 1965, pp. 54-111.
14. **Cermak J.E.** Wind tunnel design for physical modeling of atmospheric boundary layer // Journal of the Engineering Mechanics Division, 1981, Volume 107, pp. 623-642.
15. **Rofail A.W., Kwok K.C.S.** A reliability study of wind tunnel results for cladding pressures // J. Wind Eng. Ind. Aerodyn., 1992, Volume 44, Issues 1-3, pp. 2413-2424.
16. **Cochran L., Derickson R.** A physical modeler's view of computational wind engineering // J. Wind Eng. Ind. Aerodyn., 2011, Volume 99, Issue 4, pp. 139-153.
17. **Meroney R.N., Derickson R**. Virtual reality in wind engineering: the windy world within the computer // J. Wind Eng., 2014, Volume 11, pp. 11-26.
18. **Blocken B**. Computational Fluid Dynamics for urban physics: Importance, scales, possibilities, limitations and ten tips and tricks towards accurate and reliable simulations // Build. Environ., 2015, Volume 91, pp. 219-245.
19. **Blocken B.** 50 years of computational wind engineering: past, present and future // J. Wind Eng. Ind. Aerodyn., 2014, Volume 129, pp. 69-102.
20. **Mochida A., Tominaga Y., Murakami S., Yoshie R., Ishihara T., Ooka R.** Comparison of various k-ε models and DSM applied to flow around a highrise building-report on AU cooperative project for CFD prediction of wind environment // Wind Struct. Int. J., 2002, Volume 5, pp. 227-244.
21. **Celik I.B., Ghia U., Roache P.J., Freitas C.J.** Procedure for estimation and reporting of uncertainty due to discretization in CFD

applications // J. Fluids Eng. Trans. ASME, 2008, Volume 130(7).
22. **Bruno L., Salvetti M.V., Ricciardelli F.** Benchmark on the aerodynamics of a rectangular 5:1 cylinder: an overview after the first four years of activity // J. Wind Eng. Ind. Aerodyn., 2014, Volume. 126, pp. 87-106.
23. **Thordal M.S., Bennetsen J.C., Capra S., Kragh A.K., Koss H.H.H.** Towards a standard CFD setup for wind load assessment of high-rise buildings: Part 2– Blind test of chamfered and rounded corner high-rise buildings // J. Wind Eng. Ind. Aerodyn., 2020, Volume 205, p. 104282.
24. **Franke J., Hellsten A., Schlünzen K.H., Carissimo B.** Best practice guideline for the CFD simulation of flows in the urban environment-a summary // 11th Conference on Harmonisation within Atmospheric Dispersion Modelling for Regulatory Purposes, Cambridge, UK, July 2007, 2007.
25. **Tominaga Y., Mochida A., Yoshie R., Kataoka H., Nozu T., Yoshikawa M., Shirasawa T.** AIJ guidelines for practical applications of CFD to pedestrian wind environment around buildings // J. Wind Eng. Ind. Aerodyn., 2008, Volume 96, Issues 10-11, pp. 1749-1761.
26. Guidebook of Recommendations for Wind Loads on Buildings 2 – Wind Induced Response and Load Estimation / Practical Guide of CFD for Wind Resistant Design, AIJ, 2017. (in Japanese)
27. CNR DT 207 R1/2018 Istruzioni per la valutazione delle azioni e degli effetti del vento sulle costruzioni, 2019. (in Italian)
28. ASCE/SEI 7-22 Minimum Design Loads and Associated Criteria for Building and other Structures, 2022.
29. Matematicheskoe (chislennoe)" modelirovanie vetrovyh nagruzok i vozdejstvij. Metodicheskoe posobie. Moscow: FAU «FCS», 2020, 61 p.
30. SP 20.13330.2016 Loads and actions (with changes №1-4). Moscow: FGBU «RST» 2022.
31. **Belostotsky A.M., Akimov P.A., Afanasyeva I.N.** Vychislitel'naya aerodinamika v zadachah stroitel'stva, Moscow: Izdatel'stvo ASV, 2017, 720 p. (in Russian).
32. **Britikov N.A**. Numerical modelling of snow deposits and snow transport on long-span roofs for steady and unsteady flow // International Journal for Computational Civil and Structural Engineering, 2022, Volume 18(4), pp. 23–38.
33. **Belostotsky A.M., Afanasyeva I.N., Negrozova I.Yu., Goryachevsky O.S**. Simulation of aerodynamic instability of building structures on the example of a bridge section. Part 2: solution of the problem in a coupled aeroelastic formulation and comparison with engineering estimates // International Journal for Computational Civil and Structural Engineering, 2021, Volume 17(3), pp. 24-38.
34. **Belostotsky A.M., Afanasyeva I.N., Lantsova I.Yu.** Estimation of pedestrian comfort on the basis of numerical modeling of wind aerodynamics of buildings in the environmental development // International Journal for Computational Civil and Structural Engineering, 2019, Volume 15(2), pp. 24-39.
35. **Menter F.R.** Review of the shear-stress transport turbulence model experience from an industrial perspective // J. Wind Eng. Ind. Aerodyn., 2009, Volume 23, pp. 305-316.
36. **Menter F.R.** Best Practice: Scale-Resolving Simulations in ANSYS CFD. Version 2.00. Technical paper. ANSYS, 2015, 47 p.
37. **Menter F., Hüppe A., Matyushenko A., Kolmogorov D.** An overview of hybrid RANS–LES models developed for industrial CFD // Appl. Sci., 2021, Volume 11, p. 2459, 2021.
38. **Oberkampf W.L., Trucano T.G., Hirsch C**. Verification, validation, and predictive capability in computational engineering and

physics // Appl. Mech. Rev., 2004, Volume 57, pp. 345-384.

39. **Meroney R.N.** Ten questions concerning hybrid computational/physical model simulation of wind flow in the built environment // Build. Environ., 2016, Volume 96, pp. 12-21.
40. **Menter F., Lechner R., Matyushenko A.** Best practice: Generalized k-ω (GEKO) Two-Equation Turbulence Model in ANSYS CFD: Version 1.01. Best Practice. ANSYS, 2019, 32 p.
41. **Sharkey P.S., Menter F.R.** A numerical investigation of the turbulent flow around a scale model JBC hull using the Generalized k-omega (GEKO) turbulence model // 11th International Workshop on Ship and Marine Hydrodynamics (IWSH2019), 2019.
42. **Kok J.C.** Resolving the Dependence on Freestream Values for the k-omega Turbulence Model // AIAA Journal, 2000, Volume 38(7), pp. 1292-1295.

СПИСОК ЛИТЕРАТУРЫ

1. **Казакевич М.И.** Аэродинамика инженерных сооружений. Москва: ОАО Гипростроймост, 2014, 168 с.
2. **Cermak J.E., Koloseus H.J.** Lake Hefner Model Studies of Wind Structure and Evaporation. Final Report – Part II, № 54JEC22, 1954, 123 p.
3. **Davenport A.G.** The response of supertall buildings to wind // Second Century of the Skyscraper: Council on Tall Buildings and Urban Habitat, 1988, pp. 705-725.
4. **Glanz J., Lipton E.** City in the Sky: The Rise and Fall of the World Trade Center. Times Books, 2014, 480 p.
5. **Rathbun J.C.** Wind forces on a tall building // Trans. Am. Soc. Civil Eng., 1940, Volume 105, pp. 1-41.
6. **Marshall R.D**. A study of wind pressures on a single-family dwelling in model and full scale // J. Wind Eng. Ind. Aerodyn., 1975, Volume 1, pp. 177-199.
7. **Eaton K.J., Mayne J.R.** The measurement of wind pressures on two-storey houses at Aylesbury // J. Wind Eng. Ind. Aerodyn., 1975, Volume 1, pp. 67-109.
8. **Holmes J.D**. Comparison of model and full-scale tests of the Aylesbury house // Proceedings of the International Workshop on Wind Tunnel Modeling Criteria and Techniques in Civil Engineering Applications, 1982, pp. 605-618.
9. **Richardson G.M., Robertson A.P., Hoxey R.P., Surry D.** Full-scale and model investigations of pressures on an industrial/agricultural building // J. Wind Eng. Ind. Aerodyn., 1990, Volume 36(2), pp. 1053-1062.
10. **Hoxey R.P., Richards P.J.** Full-scale wind load measurements point the way forward // J. Wind Eng. Ind. Aerodyn, 1995, Volume 57, Issues 2-3, pp. 215-224.
11. **Монин А.С., Обухов А.М.** Основные закономерности турбулентного перемешивания в приземном слое атмосферы // Труды ГЕОФИАН, 1954. № 24 (151), с. 163-187
12. **Van der Hoven I.** Power spectrum of horizontal wind speed in the frequency range from 0.0007 to 900 cycles per hour // Journal of Atmospheric Sciences, 1957 Volume 14, pp. 160-164.
13. **Davenport A.G.** The relationship of wind structure to wind loading // Proc. Conf. on Wind Effects on Buildings & Structures, HMSO, 1965, pp. 54-111.
14. **Cermak J.E**. Wind tunnel design for physical modeling of atmospheric boundary layer // Journal of the Engineering Mechanics Division, 1981, Volume 107, pp. 623-642.
15. **Rofail A.W., Kwok K.C.S.** A reliability study of wind tunnel results for cladding pressures // J. Wind Eng. Ind. Aerodyn., 1992, Volume 44, Issues 1-3, pp. 2413-2424.
16. **Cochran L., Derickson R.** A physical modeler's view of computational wind

engineering // J. Wind Eng. Ind. Aerodyn., 2011, Volume 99, Issue 4, pp. 139-153.

17. Meroney R.N., Derickson R. Virtual reality in wind engineering: the windy world within the computer // J. Wind Eng., 2014, Volume 11, pp. 11-26.
18. **Blocken B.** Computational Fluid Dynamics for urban physics: Importance, scales, possibilities, limitations and ten tips and tricks towards accurate and reliable simulations // Build. Environ., 2015, Volume 91, pp. 219-245.
19. **Blocken B.** 50 years of computational wind engineering: past, present and future // J. Wind Eng. Ind. Aerodyn., 2014, Volume 129, pp. 69-102.
20. **Mochida A., Tominaga Y., Murakami S., Yoshie R., Ishihara T., Ooka R.** Comparison of various k-ε models and DSM applied to flow around a highrise building-report on AU cooperative project for CFD prediction of wind environment // Wind Struct. Int. J., 2002, Volume 5, pp. 227-244.
21. **Celik I.B., Ghia U., Roache P.J., Freitas C.J.** Procedure for estimation and reporting of uncertainty due to discretization in CFD applications // J. Fluids Eng. Trans. ASME, 2008, Volume 130(7).
22. **Bruno L., Salvetti M.V., Ricciardelli F**. Benchmark on the aerodynamics of a rectangular 5:1 cylinder: an overview after the first four years of activity // J. Wind Eng. Ind. Aerodyn., 2014, Volume. 126, pp. 87-106.
23. **Thordal M.S., Bennetsen J.C., Capra S., Kragh A.K., Koss H.H.H.** Towards a standard CFD setup for wind load assessment of high-rise buildings: Part 2– Blind test of chamfered and rounded corner high-rise buildings // J. Wind Eng. Ind. Aerodyn., 2020, Volume 205, p. 104282.
24. **Franke J., Hellsten A., Schlünzen K.H., Carissimo B**. Best practice guideline for the CFD simulation of flows in the urban environment-a summary // 11th Conference on Harmonisation within Atmospheric Dispersion Modelling for Regulatory Purposes, Cambridge, UK, July 2007, 2007.
25. **Tominaga Y., Mochida A., Yoshie R., Kataoka H., Nozu T., Yoshikawa M., Shirasawa T.** AIJ guidelines for practical applications of CFD to pedestrian wind environment around buildings // J. Wind Eng. Ind. Aerodyn., 2008, Volume 96, Issues 10-11, pp. 1749-1761.
26. Guidebook of Recommendations for Wind Loads on Buildings 2 – Wind Induced Response and Load Estimation / Practical Guide of CFD for Wind Resistant Design, AIJ, 2017. (in Japanese)
27. CNR DT 207 R1/2018 Istruzioni per la valutazione delle azioni e degli effetti del vento sulle costruzioni, 2019. (in Italian)
28. ASCE/SEI 7-22 Minimum Design Loads and Associated Criteria for Building and other Structures, 2022.
29. Математическое (численное)" моделирование ветровых нагрузок и воздействий. Методическое пособие, М.: ФАУ «ФЦС», 2020, 61 с.
30. СП 20.13330.2016 Нагрузки и воздействия. Актуализированная редакция СНиП 2.01.07-85* (с Изменениями N 1, 2, 3, 4), М.: ФГБУ «РСТ», 2022.
31. **Белостоцкий А.М., Акимов П.А., Афанасьева И.Н.** Вычислительная аэродинамика в задачах строительства, М.: Издательство АСВ, 2017, 720 с.
32. **Бритиков Н.А.** Методика численного моделирования снегоотложений и снегопереноса на покрытиях большепролётных зданий и сооружений в стационарной и нестационарной постановках // International Journal for Computational Civil and Structural Engineering, 2022, Том 18(4), с. 23–38.
33. **Белостоцкий А.М., Афанасьева И.Н., Негрозова И.Ю., Горячевский О.С.** Моделирование аэродинамической неустойчивости строительных конструкций на примере сечения моста. Часть 2: Решение задачи в связанной

аэроупругой постановке и сопоставление с инженерными оценками // International Journal for Computational Civil and Structural Engineering, 2021, Том 17(3), с. 24-38.
34. **Белостоцкий А.М., Афанасьева И.Н., Ланцова И.Ю**. Оценка пешеходной комфортности на основе численного моделирования ветровой аэродинамики зданий в окружающей застройке // International Journal for Computational Civil and Structural Engineering, 2019, Том 15(2), с. 24-39.
35. **Menter F.R.** Review of the shear-stress transport turbulence model experience from an industrial perspective // J. Wind Eng. Ind. Aerodyn., 2009, Volume 23, pp. 305-316.
36. **Menter F.R.** Best Practice: Scale-Resolving Simulations in ANSYS CFD. Version 2.00. Technical paper. ANSYS, 2015, 47 p.
37. **Menter F., Hüppe A., Matyushenko A., Kolmogorov D.** An overview of hybrid RANS–LES models developed for industrial CFD // Appl. Sci., 2021, Volume 11, p. 2459, 2021.
38. **Oberkampf W.L., Trucano T.G., Hirsch C.** Verification, validation, and predictive capability in computational engineering and physics // Appl. Mech. Rev., 2004, Volume 57, pp. 345-384.
39. **Meroney R.N.** Ten questions concerning hybrid computational/physical model simulation of wind flow in the built environment // Build. Environ., 2016, Volume 96, pp. 12-21.
40. **Menter F., Lechner R., Matyushenko A**. Best practice: Generalized k-ω (GEKO) Two-Equation Turbulence Model in ANSYS CFD: Version 1.01. Best Practice. ANSYS, 2019, 32 p.
41. **Sharkey P.S., Menter F.R.** A numerical investigation of the turbulent flow around a scale model JBC hull using the Generalized k-omega (GEKO) turbulence model // 11th International Workshop on Ship and Marine Hydrodynamics (IWSH2019), 2019.
42. **Kok J.C.** Resolving the Dependence on Freestream Values for the k-omega Turbulence Model // AIAA Journal, 2000, Volume 38(7), pp. 1292-1295.

Goryachevsky Oleg Sergeevich, Deputy Director at A.B. Zolotov REC CM of the National Research Moscow State University of Civil Engineering; 129337, Russia, Moscow, Yaroslavskoe shosse, 26.
E-mail: osgoryachevskij@mail.ru

Горячевский Олег Сергеевич, заместитель директора НОЦ КМ им. А.Б. Золотова Национального исследовательского Московского государственного строительного университета; 129337, Россия, г. Москва, Ярославское шоссе, д. 26.
E-mail: osgoryachevskij@mail.ru